Cell Metabolism
Article

# A Switch from White to Brown Fat Increases Energy Expenditure in Cancer-Associated Cachexia

Michele Petruzzelli,[1] Martina Schweiger,[2] Renate Schreiber,[2] Ramon Campos-Olivas,[3] Maria Tsoli,[4] John Allen,[5] Michael Swarbrick,[5] Stefan Rose-John,[6] Mercedes Rincon,[7] Graham Robertson,[5] Rudolf Zechner,[2] and Erwin F. Wagner[1,*]

[1]BBVA Foundation-CNIO Cancer Cell Biology Programme, Spanish National Cancer Research Centre (CNIO), C/ Melchor Fernández Almagro 3, 28029 Madrid, Spain
[2]Institute of Molecular Biosciences, University of Graz, Humboldtstrasse 50, 8010 Graz, Austria
[3]Spectroscopy and Nuclear Magnetic Resonance Unit, Spanish National Cancer Research Centre (CNIO), C/ Melchor Fernández Almagro 3, 28029 Madrid, Spain
[4]Children's Cancer Institute Australia for Medical Research, UNSW Lowy Cancer Research Centre Building, C25 Kensington Campus UNSW, Sydney, NSW 2052, Australia
[5]Garvan Institute of Medical Research, 384 Victoria Street, Darlinghurst, NSW 2010, Australia
[6]Institute of Biochemistry, Christian-Albrechts University, Olshausenstr. 40, 24118 Kiel, Germany
[7]Division of Immunobiology, Department of Medicine, University of Vermont, 89 Beaumont Avenue / D305 Given Building, Burlington, VT 05405, USA
*Correspondence: ewagner@cnio.es
http://dx.doi.org/10.1016/j.cmet.2014.06.011

## SUMMARY

**Cancer-associated cachexia (CAC) is a wasting syndrome characterized by systemic inflammation, body weight loss, atrophy of white adipose tissue (WAT) and skeletal muscle. Limited therapeutic options are available and the underlying mechanisms are poorly defined. Here we show that a phenotypic switch from WAT to brown fat, a phenomenon termed WAT browning, takes place in the initial stages of CAC, before skeletal muscle atrophy. WAT browning is associated with increased expression of uncoupling protein 1 (UCP1), which uncouples mitochondrial respiration toward thermogenesis instead of ATP synthesis, leading to increased lipid mobilization and energy expenditure in cachectic mice. Chronic inflammation and the cytokine interleukin-6 increase UCP1 expression in WAT, and treatments that reduce inflammation or β-adrenergic blockade reduce WAT browning and ameliorate the severity of cachexia. Importantly, UCP1 staining is observed in WAT from CAC patients. Thus, inhibition of WAT browning represents a promising approach to ameliorate cachexia in cancer patients.**

## INTRODUCTION

Cancer-associated cachexia (CAC) is a paraneoplastic syndrome characterized by systemic inflammation, body weight loss, atrophy of adipose tissue, and skeletal muscle wasting. CAC is observed in a majority of cancer patients with advanced disease (Fearon et al., 2012; Tisdale, 2002). In addition to cancer patients, cachexia is typically seen at the end stage of various other morbidities, including infectious diseases, such as AIDS and tuberculosis, or chronic conditions, such as congestive heart failure, chronic obstructive lung disease, and multiple sclerosis (Tisdale, 2009). No effective treatment is currently available for cachexia, which is responsible for approximately 20% of total deaths in cancer patients (Fearon et al., 2013). Therefore, new therapeutic targets for cachexia prevention and treatment are urgently needed.

Metabolic dysfunction and increased metabolic rate have been proposed as causative for CAC (Blum et al., 2011), but the underlying mechanisms are at present poorly characterized (Tisdale, 2009). Activation of thermogenesis in the interscapular brown adipose tissue (BAT) has been observed in a syngeneic mouse tumor transplant model and suggested to contribute to the hypermetabolic state of cachexia (Tsoli et al., 2012). White adipose tissue (WAT) and BAT usually perform opposite physiological functions, with WAT responsible for energy accumulation in intracellular lipid droplets and BAT responsible for its dissipation as heat (Cannon and Nedergaard, 2004). Interscapular BAT is not the only thermogenic organ in mice and humans. Brown adipocytes can also be induced within WAT depots, a phenomenon termed WAT browning (Wu et al., 2013; Young et al., 1984). Brown adipocytes induced in WAT, also known as "beige" or "brite" cells (Harms and Seale, 2013), are derived from a precursor population distinct from both mature white and brown adipocytes (Wang et al., 2013). Several mechanisms have been proposed for WAT browning (Villarroya and Vidal-Puig, 2013), including prolonged cold exposure (Loncar et al., 1986), adrenergic activation (Cao et al., 2011), the myokine Irisin (Boström et al., 2012), and the prostaglandin synthesis enzyme cyclooxygenase (COX) 2 (Vegiopoulos et al., 2010). WAT browning is responsible for a significant increase in total energy expenditure (Shabalina et al., 2013), and stimulation of browning has therapeutic potential to promote body fat reduction (Yoneshiro et al., 2013).

WAT atrophy represents one of the hallmarks of cachexia and is caused by β-adrenergic activation and/or inflammatory cytokine-induced lipolysis (Das et al., 2011; Fearon et al., 2012). Notably, β-adrenergic stimulation is also responsible for WAT

browning during cold acclimation (Cao et al., 2011). Furthermore, several activators of interscapular BAT also promote WAT browning (Wu et al., 2013). Since the β-adrenergic pathway is active during cachexia, and increased thermogenesis in BAT has been observed in cachectic mice (Tsoli et al., 2012), we set out to investigate whether WAT browning occurs and to analyze its impact on CAC pathophysiology. WAT browning was observed in different model systems, indicating that it is a consistent feature of cachexia. WAT browning during CAC contributed to the systemic increase in energy expenditure and promoted the wasting syndrome. Decreasing WAT browning by silencing tumor production of interleukin-6 (IL-6) or pharmacological approaches employing an anti-IL-6 monoclonal antibody, a β3-adrenergic receptor antagonist, or the nonsteroidal anti-inflammatory drug sulindac ameliorated the severity of cachexia. Importantly, browning of adipose tissue was observed in samples from cancer cachexia patients, thus underlining the translational value of our findings.

## RESULTS

### Browning of Subcutaneous WAT Is a Consistent Finding in Mouse Models of CAC

A systematic morphological analysis of WAT depots in different mouse models of CAC led to the identification of a robust phenotypic switch from white to brown fat in subcutaneous WAT of cachectic mice. Genetically engineered mouse models (GEMMs) of lung and pancreatic cancer, Kras-lung cancer GEMM (Puyol et al., 2010), and Kras-pancreatic cancer GEMM (Hingorani et al., 2005), respectively, at the age of 6–8 months displayed a loss of more than 15% of total body weight, when compared to littermate controls (Figure 1A). At necropsy, GEMMs of cancer exhibited massive fat atrophy, as evidenced by complete loss of gonadal WAT (Figure 1B). Histological examination of subcutaneous inguinal and axillary WAT, also termed anterior subcutaneous WAT (Waldén et al., 2012), revealed the presence of abundant islets composed of small adipocytes with big nuclei, multilocular cytoplasm, and positive staining for the uncoupling protein-1 (UCP1) (Figures 1C and 1D). WAT browning was also evident in a third GEMM of CAC; K5-SOS mice with skin tumors (Sibilia et al., 2000) displayed increased UCP1 staining in subcutaneous WAT as well as in the residual gonadal WAT (Figure S1A, available online). Next, we investigated WAT morphology and UCP1 protein in a chemical model of liver carcinogenesis; 19 months after injection of the carcinogen diethylnitrosamine (DEN), 50% of mice became cachectic (Figure S1B) and exhibited morphological evidence of subcutaneous WAT browning (Figure 1E).

WAT browning was also observed in murine syngeneic graft models. At 2 weeks after injection of B16 melanoma cells or Lewis lung carcinoma (LLC) cells, mice lost 25% of gonadal WAT mass, while total body weight was reduced only in the graft model with B16 cells (Figures S1C and S1D). Although the severity of cachexia in the syngeneic graft models was milder compared to cachexia observed in the tumor GEMMs, subcutaneous WAT from mice in both graft models displayed evidence of WAT browning, as shown by increased UCP1 staining and decreased lipid droplet size (Figures 1F, 1G, S1E, and S1F). Lastly, WAT morphology was investigated in a xenogeneic graft model of human cancer. Two tumor samples, Panc34 and Panc42, were obtained from distinct pancreatic cancer patients and implanted subcutaneously in immunocompromised SCID mice with a defective lymphocyte response. At 3 months after implantation, mice from both groups grew xenograft tumors of similar size, lost more than 15% of total body weight, and displayed evidence of browning of subcutaneous WAT (Figures S1G–S1I). These data obtained in very diverse experimental models of cancer show that WAT browning represents a consistent finding in CAC.

### WAT Browning Is an Early Event in the Pathophysiology of CAC

To investigate the kinetics of WAT browning and to determine whether it contributes to the wasting process in CAC, we focused on the K5-SOS mouse model of skin tumors, in which the temporal development of cachexia is rapid and reproducible. At 5 weeks of age, K5-SOS mice did not show evidence of loss of total body weight or skeletal muscle mass, but they exhibited increased spleen weight and a 50% reduction in gonadal WAT mass (precachectic mice) (Figures 2A and 2B). However, unequivocal signs of cachexia were evident in K5-SOS mice at 7 weeks of age, with significant total body weight loss (Figure 2A), anemia (Figures S2A and S2B), nearly complete atrophy of gonadal WAT, and a 50% reduction in skeletal muscle mass (Figures 2B and S2C–S2E). At the molecular level, changes described in skeletal muscle of cachectic mice (Zhou et al., 2010), such as increased nuclear staining of phospho-SMAD2, increased expression of the cell-cycle inhibitor *p21*, the proapoptotic gene *Bax*, and the proinflammatory cytokine interleukin-6 (*IL-6*), were observed in skeletal muscle of K5-SOS mice (Figures S2F and S2G). Also, increased activation of interscapular BAT was observed in cachectic mice (Figure S2H).

Remarkably, WAT browning was already detectable in precachectic mice and increased as cachexia developed (Figures 2C and 2D). *Ucp1* mRNA was upregulated in both inguinal and axillary WAT from cachectic K5-SOS mice, along with established molecular markers of browning, such as *Pgc1α*, *Pparγ*, *Cidea*, and *Prdm16* (Figures 2E and 2F). Browning of subcutaneous WAT in cachectic mice was associated with increased mitochondrial content and oxygen consumption (Figures 2G and 2H). Similarly, total levels of mitochondrial protein NDUFS1 were increased in subcutaneous WAT of cachectic mice (Figures S2I and S2J). Analysis of established expression signatures for beige-selective and brown-selective genes (Wu et al., 2012) showed a consistent increase of brown-selective markers in subcutaneous WAT of cachectic mice (Figures S3A and S3B). Furthermore, the percentage of proliferating cells was doubled in subcutaneous WAT of cachectic mice, when compared to controls (Figure S3C). Recent studies have shown that newly induced beige/brite adipocytes, induced in WAT by cold exposure or adrenergic β3-agonist treatment, arise by recruitment and de novo differentiation of progenitor cells (Wang et al., 2013). To better characterize the identity of proliferating cells in WAT of cachectic mice, we performed costaining experiments with established markers of adipocyte progenitors (Lee et al., 2012; Tang et al., 2011) and identified proliferating PDGFRα-positive cells, but not PDGFRβ or PPARγ cells (Figure S3D). These data show that WAT browning represents an early event

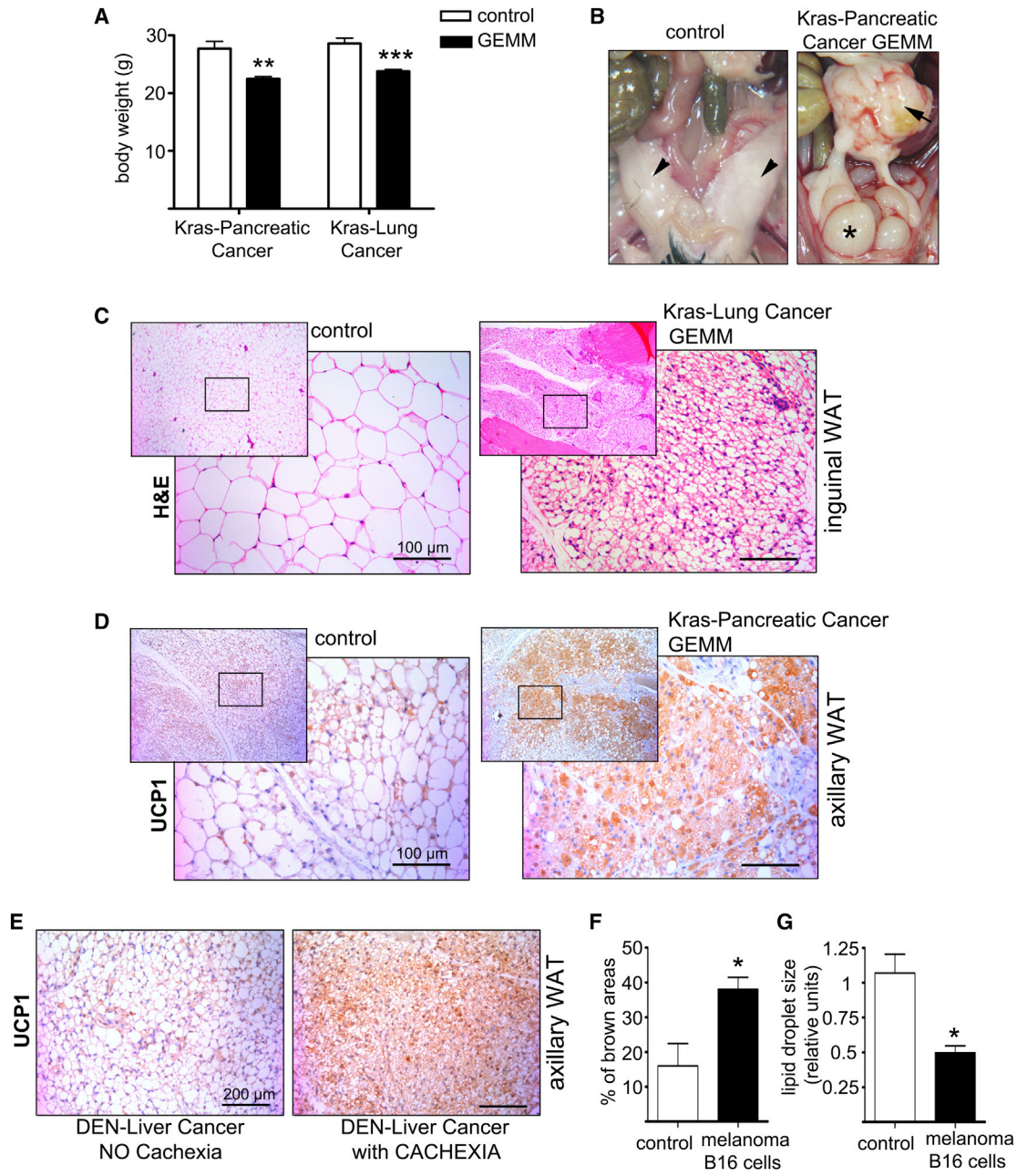


**Figure 1. Browning of WAT Is a Consistent Finding in Mouse Models of CAC**

(A) Total body weight in Kras-pancreatic cancer GEMM, Kras-lung cancer GEMM, and corresponding littermate controls (6–8 months old, n ≥ 6 per genotype).

(B) Representative macroscopic pictures of control mice and Kras-pancreatic cancer GEMM at autopsy. The arrowheads point to normal gonadal WAT in control mice. In the GEMM of pancreatic cancer (arrow), gonadal WAT is almost completely absent, and the gonads are visible (asterisk).

(C and D) Representative images of hematoxylin and eosin (H&E) (C) and UCP1 immunohistochemical (IHC) (D) staining of subcutaneous WAT in mice from (A).

(E) Representative images of UCP1 IHC staining of axillary WAT in mice in the DEN-induced model of liver tumors (16–18 months old, n = 3 per condition).

(F and G) Quantification of brown area extension (F) and lipid droplet size (G) in axillary WAT from mice in the graft model with melanoma B16 cells (12 weeks old, n ≥ 6 per condition).

Data are presented as mean ± SEM (*p < 0.05).

in the pathophysiology of cachexia, preceding skeletal muscle wasting. Moreover, WAT browning is associated with increased energy consumption in subcutaneous WAT and is characterized by activation of brown-selective genes and proliferation of PDGFRα progenitor cells.

## Increased Systemic Energy Expenditure in Cachectic K5-SOS Mice

To determine the impact of WAT browning on systemic metabolism, we studied metabolic parameters in tumor-bearing mice. Precachectic K5-SOS mice (5 weeks old) were placed in

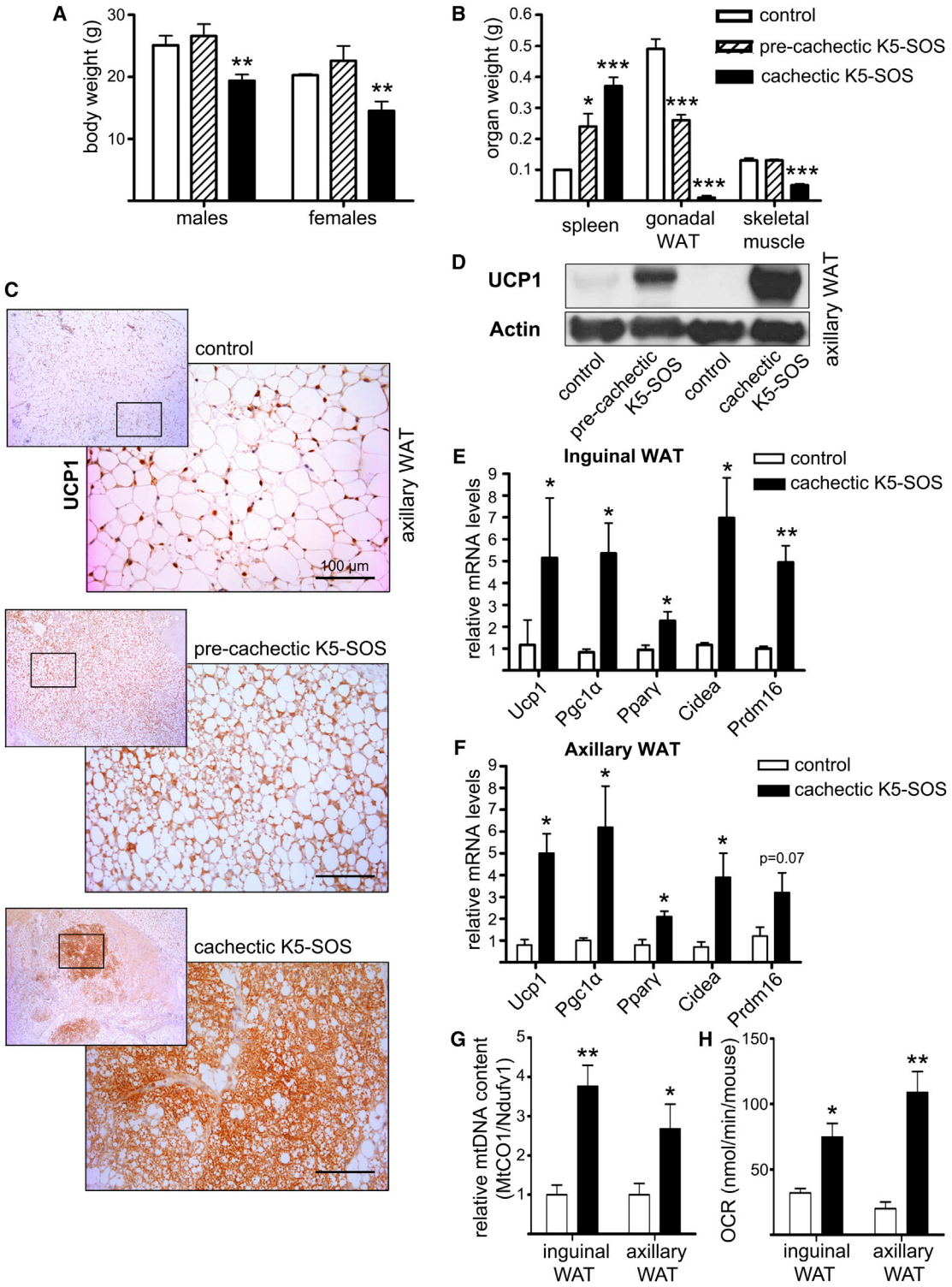


**Figure 2. Browning of WAT Is an Early Event in the Pathophysiology of CAC**

(A and B) Changes in total body (A) and organ (B) weight in 5-week-old (precachectic) and 7-week-old (cachectic) K5-SOS mice and littermate controls.

(C and D) Representative images of UCP1 IHC staining (C) and western blot analysis (D) of axillary WAT.

(E and F) Gene expression analysis of browning markers in inguinal (E) and axillary (F) WAT.

(G and H) Analysis of mitochondrial DNA content (G) and oxygen consumption rate (OCR) (H) in isolated inguinal and axillary WAT.

For all panels, n ≥ 8 per genotype and per group. Data are presented as mean ± SEM (*p < 0.05; **p < 0.01; ***p < 0.001).

metabolic cages and examined for 2 weeks. Energy expenditure (EE) progressively increased in K5-SOS mice over this time in both diurnal and nocturnal periods and reached significantly increased values during the last 3 days, when mice were overtly cachectic (Figures 3A and 3B). Respiratory exchange ratios (RERs) were reduced in K5-SOS mice, highlighting the importance of lipids as the primary fuel source in cachectic mice (Figures 3C and 3D). Food intake was increased in cachectic mice (Figure 3E), yet feeding a high-fat diet did not prevent loss of total body weight or tissue atrophy (Figures S4A and S4B). Notably, energy expenditure was increased in cachectic mice despite reduced locomotor activity (Figure 3F).

Increased glucose recycling via lactate, a metabolic pathway termed the Cori cycle, has been described in cachectic cancer patients and suggested to play a causal role in the increased energy expenditure (Holroyde et al., 1984; Tisdale, 2009). To analyze a possible contribution of the Cori cycle to the cachectic phenotype observed in K5-SOS mice, the levels of substrates for gluconeogenesis were measured by NMR in plasma and tissue extracts from liver and skeletal muscle. Although significantly increased levels of alanine (plasma and liver) and pyruvate (liver) were detected in cachectic mice, which may suggest enhanced Cori cycle activity, these increases were not accompanied by a corresponding increase in lactate levels, which remained unchanged and of much higher magnitude (Figures S4C–S4E). Furthermore, expression levels of key enzymes, transporters, and transcription factors involved in lactate metabolism (Summermatter et al., 2013) were similar in liver and skeletal muscle from K5-SOS and control mice (Figures S4F and S4G), indicating that the Cori cycle is not significantly active in this cachectic model.

Atrophy of gonadal WAT in K5-SOS mice was associated with increased triglyceride hydrolase activity due to increased activity of adipose triglyceride lipase (ATGL) and hormone-sensitive lipase (HSL), as confirmed by the reduction in fatty acid and glycerol release from gonadal WAT explants after addition of the respective lipase inhibitor (Figures 3G and 3H). Interestingly, while inhibition of ATGL and HSL led to a reduction greater than 85% in fatty acid and glycerol release from gonadal WAT of control mice (86% and 97% reduction, respectively), the fold reduction after lipase inhibitors was considerably less for K5-SOS mice (60% and 67% reduction, respectively), indicating that higher doses of inhibitors are required to counteract lipolysis during cachexia. Alternatively, other yet-unidentified lipases may become active and contribute to triacylglycerol hydrolysis and WAT loss in cachexia. Increased lipolysis was also evident in inguinal and axillary WAT (Figure 3I) due to pronounced overexpression of adipose ATGL, HSL, and phospho-HSL (Figure 3J). The increase in lipid mobilization and energy expenditure despite decreased locomotor activity suggests that WAT browning, together with enhanced thermogenesis in interscapular BAT, contributes to excessive substrate oxidation and wasting in CAC.

## Role of Inflammation in the Pathophysiology of WAT Browning in Cachexia

Although it is established that WAT browning enhances thermogenesis (Cousin et al., 1992), rectal temperature was reduced in 7-week-old cachectic K5-SOS mice housed at standard temperatures (23°C) (Figure S5A). To evaluate whether WAT browning represents a defense mechanism against lower body temperature (Wu et al., 2013), mice were kept at thermoneutrality (30°C) starting at 4 weeks of age. Housing mice at thermoneutrality for 1 month did not affect the loss of WAT and skeletal muscle mass and did not rescue the reduction in body temperature or the WAT browning phenotype (Figures S5B–S5E). These data show that WAT browning in cachectic mice is independent of environmental thermal stimuli.

Searching for a common cause of WAT browning in all analyzed models of CAC, we reasoned that chronic inflammation would be a good candidate, since it is a hallmark of both clinical (Blum et al., 2011) and experimental CAC (Fearon et al., 2012). In order to define the potential role of inflammation in the pathogenesis of the WAT browning phenotype, we examined inflammation-induced signaling pathways in WAT of mice with the K5-SOS, Kras-pancreatic cancer GEMM, and colon carcinoma C26 syngeneic tumors (Tsoli et al., 2012). In all three models, STAT3 was activated, and phosphorylation of the MAPK p38 was increased in WAT of K5-SOS and C26 mice (Figures S6A–S6C). Increased expression of *Socs3*, downstream of STAT3, and *Cox1*, indicative of enhanced prostaglandin signaling, was observed (Figures S6D and S6E). Furthermore, systemic chronic inflammation was documented by leukocytosis with increased neutrophil/lymphocyte ratio (Figures S6F and S6G) and fibrosis of subcutaneous WAT and liver (Figures S6H–S6K). Notably, cachectic mice displayed increased IL-6 levels in blood (Figure S6L).

IL-6 is a proinflammatory cytokine with a major role in cachexia pathophysiology (Fearon et al., 2012). To further delineate the role of IL-6 in promoting WAT browning, we employed C26 carcinoma cells, which are IL-6 proficient, as well as a C26 tumor variant that lacks IL-6. Although the syngeneic tumor from IL-6-proficient C26 cells was smaller compared to the tumor from IL-6-deficient C26 cells (Figure 4A), only mice injected with IL-6-proficient C26 cells rapidly lost body weight and became cachectic (Figures 4B and 4C). Likewise, UCP1 protein content was high only in subcutaneous WAT of mice implanted with IL-6-proficient C26 tumors (Figure 4D). To confirm the role of IL-6 in causing cachexia in the C26 colon cancer model, we blocked IL-6 expression in IL-6-proficient C26 cells by stable incorporation of an shRNA targeting IL-6. Preventing IL-6 release by C26 tumors completely rescued the cachectic phenotype (Figures 4E and 4F). Notably, silencing IL-6 in C26 tumors also blocked the increased UCP1 protein expression in subcutaneous adipose tissue (Figure 4G). In addition, the increased mitochondrial respiratory function observed in axillary WAT from mice implanted with IL-6-proficient C26 cells was partially normalized after IL-6 silencing (Figure 4H).

To further address the role of IL-6 in WAT browning, an anti-IL-6 blocking antibody was used. Anti-IL-6 treatment was started in K5-SOS mice at 5 weeks of age, when a severe reduction in total fat mass was documented by dual-energy X-ray absorptiometry (DXA) analysis (Figure S6M). Treatment for 2 weeks with anti-IL-6 monoclonal antibody prevented the further reduction of total body fat and reduced UCP1 protein levels in subcutaneous WAT (Figures 4I and 4J). Despite the beneficial effect on WAT atrophy, total body loss was not affected by anti-IL-6 treatment (Figure S6N). The partial effect could be due to the inability of

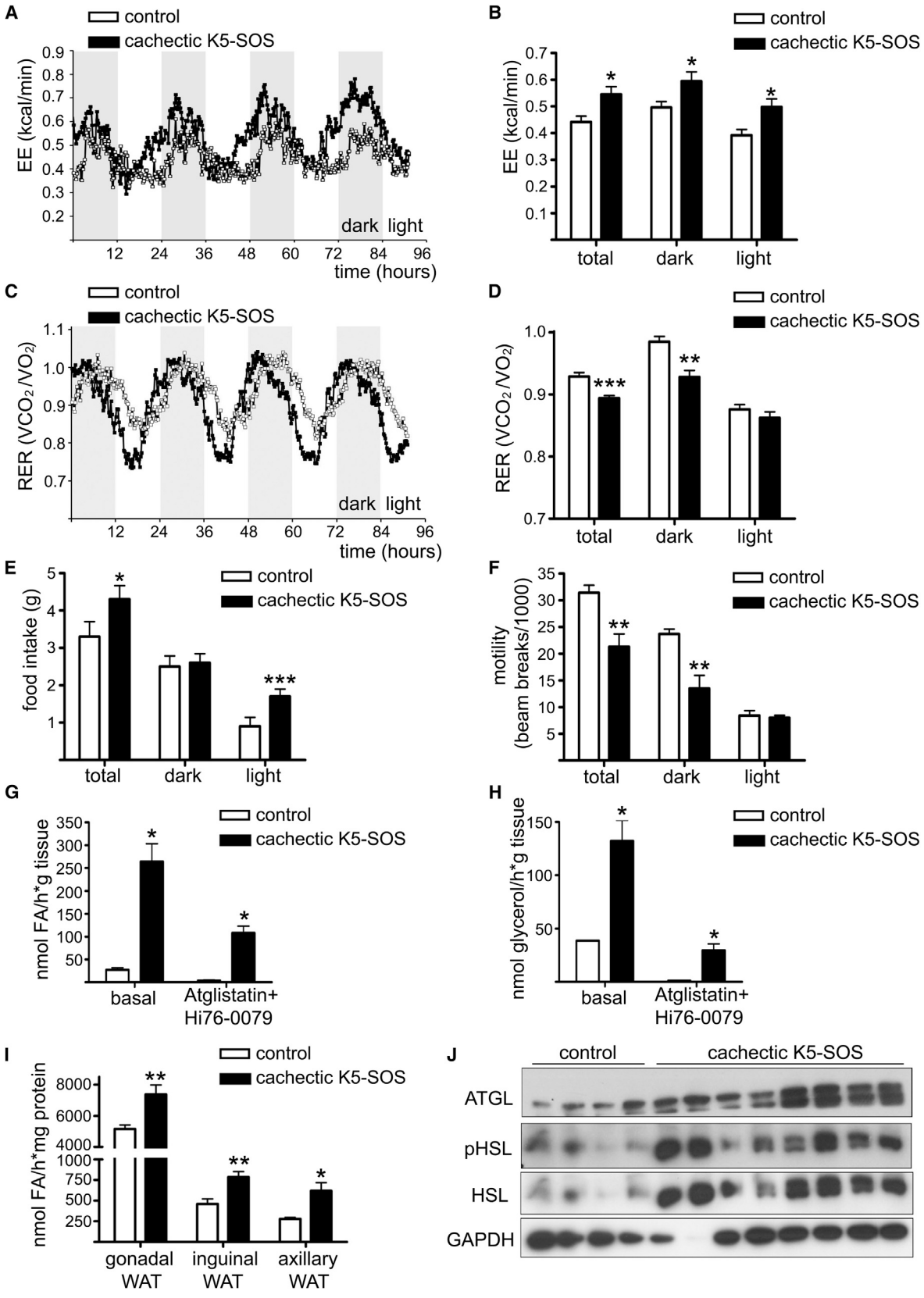


(legend on next page)

the antibody to fully neutralize IL-6. To complement these experiments, the severity of cachexia was investigated in IL-6 receptor knockout (IL-6-R-KO) mice. At 2 weeks after implantation of B16 melanomas, WAT atrophy was significantly reduced in mutant mice, although the protection against total body weight loss was small and did not reach statistical significance (Figures 4K and 4L). Importantly, UCP1 protein levels in subcutaneous WAT from IL-6-R-KO mice implanted with B16 melanoma cells were drastically reduced when compared to control mice (Figure 4M). Combined with the functional evidence for reversal of browning in the IL-6 knockdown C26 tumor model, these data establish that IL-6 signaling plays an important role in the WAT browning phenotype observed in mouse models of cachexia.

### Role of β-Adrenergic Activation in the Pathogenesis of WAT Browning in Cachectic Mice

It has recently been reported that IL-6 determines alternative activation of macrophages (Mauer et al., 2014). Interestingly, alternatively activated macrophages sustain adaptive thermogenesis in BAT through enhanced recruitment of β-adrenergic fibers (Nguyen et al., 2011). Macrophage infiltration was evident in subcutaneous WAT of mice in the syngeneic graft model with IL-6-proficient C26 cells, as well as in other models of cachexia, including K5-SOS mice and mice in the xenogeneic transplant model with human pancreatic cancer (Figure S7A and data not shown). Gene expression analysis of axillary WAT in K5-SOS mice showed increased levels of markers of the alternatively activated M2 macrophages (*IL4* and *Arg1*), while levels of the M1 marker *TNFα* were unchanged (Figure S7B). Positive immunohistochemical staining for the rate-limiting enzyme of catecholamine synthesis, tyrosine hydroxylase (TH), confirmed β-adrenergic activation in WAT of cachectic mice (Figure S7C).

To determine the role of adrenergic innervation in the induction of the thermogenic program in cachectic mice, we tested whether bilateral surgical denervation of BAT would affect the increased UCP1 protein levels observed in this tissue in K5-SOS mice. At 1 week after surgery, BAT from denervated control mice appeared pale, displayed adipocytes of bigger dimensions with less vacuolization of the cytoplasm, and showed a drastic reduction in UCP1 protein levels (Figures 5A–5D). Interestingly, in K5-SOS mice, although BAT denervation was also effective in decreasing UCP1 levels, residual protein levels were higher than those in denervated control mice (Figures 5A–5D). These data suggest that the presence of an intact adrenergic innervation is essential for the complete induction of the thermogenic program in BAT of cachectic mice. However, even in the absence of innervation, adrenergic-independent mechanisms still determine a partial increase of UCP1 protein levels.

We next tested in vitro whether IL-6 was able to directly increase *Ucp1* levels in adipocytes. We used 3T3-L1 pre-white adipocytes retrovirally transduced with Cebp/β (Ortega-Molina et al., 2012), as a model of pre-brown adipocytes, as well as primary adipocytes from inguinal WAT. Treatment with the cyclic AMP inducer Forskolin increased *Ucp1* expression levels by 8-fold and 30-fold in the cell line and in primary adipocytes, respectively (Figures S7D and S7E). Although less robust, a statistically significant increase in *Ucp1* mRNA levels was observed after treatment of both cell models with recombinant murine IL-6 (Figures S7D and S7E), thus providing evidence for a small but distinct effect of the cytokine upon *Ucp1* expression in adipocytes.

These data show that chronic inflammation together with β-adrenergic activation functionally cooperate in the pathogenesis of increased adipose tissue thermogenesis in cachexia.

### β3-Adrenergic Receptor Blockade and Anti-Inflammatory Treatment Ameliorate Cachexia

Adrenergic control of thermogenesis in adipose tissue is mediated mainly by β3-adrenergic receptors (Cao et al., 2011). To investigate the potential to prevent cachexia, treatment with the selective β3-adrenergic receptor (β3-AR) antagonist was started in mice after weaning, at 3 weeks of age, when no sign of cachexia was apparent in K5-SOS mice. Treating mice for 4 weeks with the selective β3-AR antagonist ameliorated cachexia and decreased UCP1 levels in subcutaneous WAT (Figures 6A–6C). While inhibition of β3-AR did not significantly reduce *Ucp1* mRNA expression levels in subcutaneous WAT of control mice, the treatment was effective in reducing *Ucp1* expression in K5-SOS mice (Figure 6C). Similarly, multilocular areas were reduced in subcutaneous WAT of K5-SOS mice treated with the selective β3-AR antagonist, when compared to vehicle-treated cachectic mice (Figure 6D).

The increased chronic inflammation observed in cachectic mice prompted us to treat K5-SOS mice with the nonselective COX1/2 inhibitor, nonsteroidal anti-inflammatory drug sulindac. Similarly to the experimental design with the β3-AR antagonist, the preventive potential of sulindac was tested starting the treatment at 3 weeks of age. Treating K5-SOS mice for 4 weeks with sulindac was very effective in ameliorating the severity of cachexia, along with a reduction of browning in subcutaneous WAT (Figures 6E–6H). Similarly to what was observed with the

**Figure 3. Increased Systemic Energy Expenditure and Lipid Mobilization in Cachectic Mice**

Precachectic K5-SOS mice and littermate controls (5 weeks old) were housed individually in metabolic cages and recorded during 2 weeks. Results of the last 3 days of measurement are shown, a time point at which K5-SOS mice were overtly cachectic.

(A) Energy expenditure (EE) at each time point.

(B) Average EE over the last 3 days

(C) Respiratory exchange ratio (RER) at each time point.

(D) Average RER over the last 3 days.

(E) Food intake.

(F) Overall motility.

(G and H) Fatty acid (FA) (G) and glycerol (H) release from gonadal WAT under basal conditions and after treatment with ATGL inhibitor (Atglistatin) plus HSL inhibitor (Hi76-0079).

(I) In vitro triglyceride hydrolase activity of lysates from gonadal, inguinal, and axillary WAT.

(J) Western blot analysis of ATGL, phospho-HSL, and HSL protein levels in axillary WAT.

For all panels, $n \geq 6$ per genotype. Data are presented as mean ± SEM (*$p < 0.05$; **$p < 0.01$; ***$p < 0.001$).

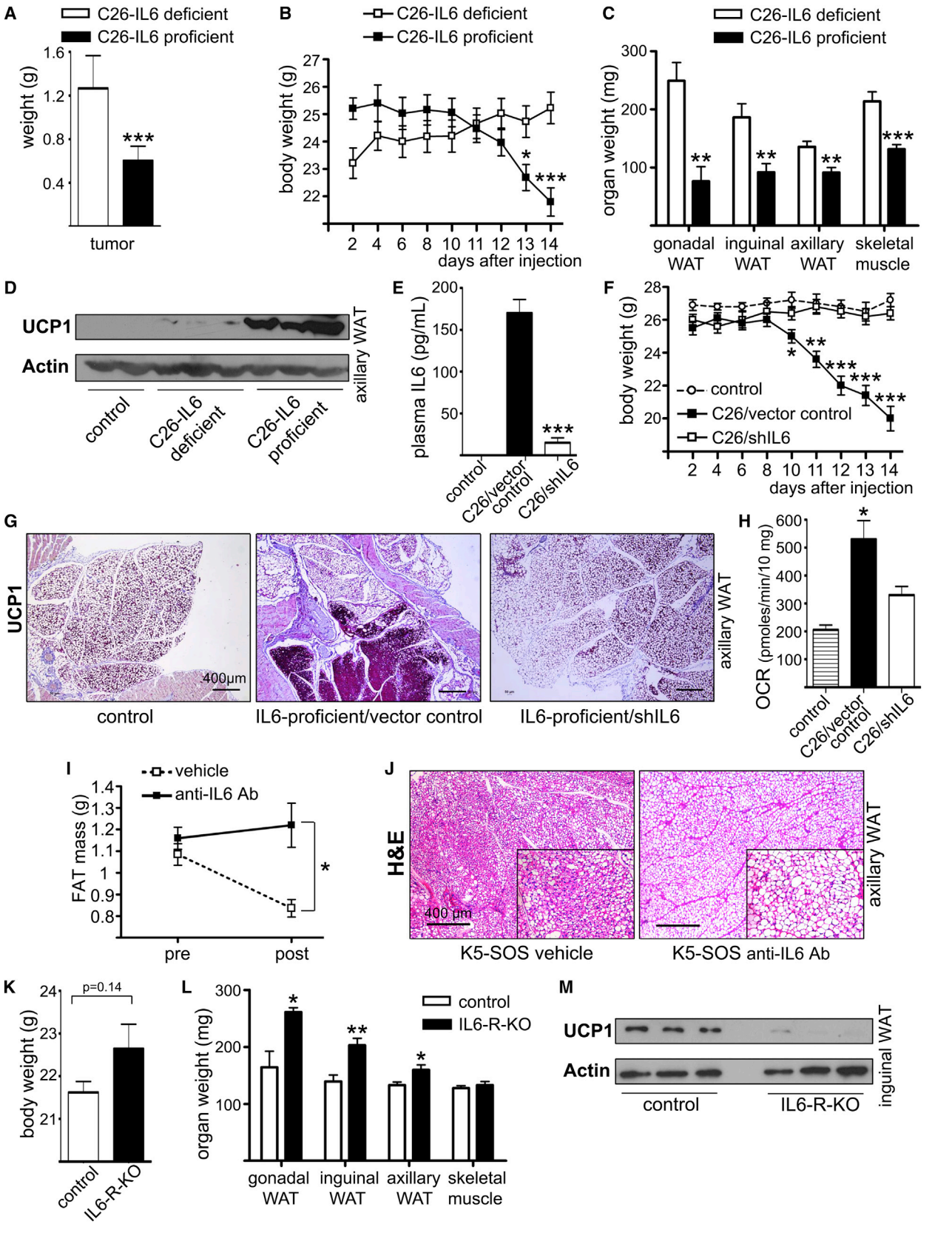


(legend on next page)

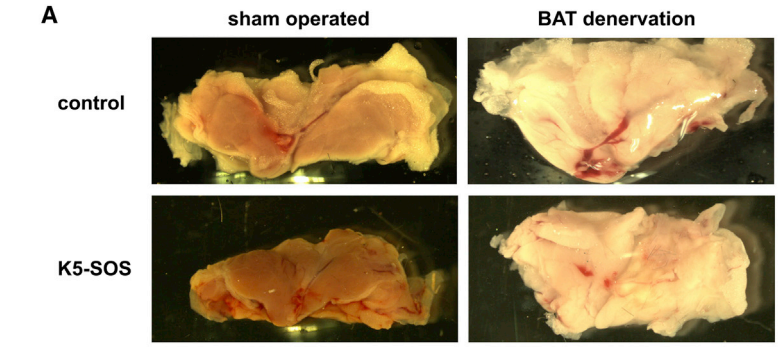


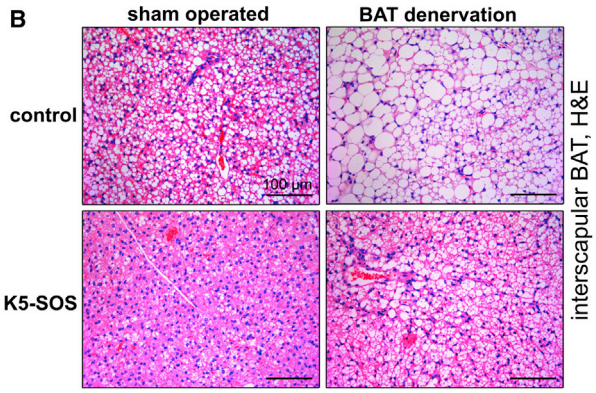


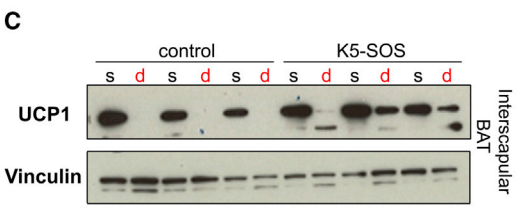


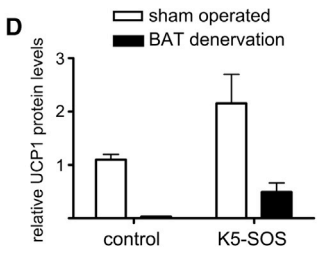


**Figure 5. Reduced UCP1 Protein Levels in Interscapular BAT after BAT Denervation in Cachectic Mice**

(A) Representative macroscopic pictures of BAT from 5-week-old K5-SOS mice and littermate controls, 1 week after bilateral BAT denervation surgery or sham operation.

(B) Representative images of H&E staining of BAT.

(C and D) Western blot analysis of UCP1 protein levels (C) and corresponding quantification (s, sham operated; d, BAT denervation) (D).

Data are presented as mean ± SEM; n = 3 per genotype and per condition.

β3-AR antagonist, sulindac treatment only reduced *Ucp1* mRNA expression levels in cachectic mice (Figure 6G). Notably, a reduction in UCP1 protein levels in WAT of sulindac-treated mice was already detected after 1 week of treatment (Figures S7F and S7G), a time point when amelioration of cachexia was not yet seen, thus showing that the reduction of WAT browning is an early effect of sulindac treatment.

These experiments show that preventive treatments are effective in ameliorating the severity of cancer cachexia and that nonsteroidal anti-inflammatory drugs are more potent than β3-AR blockade.

## UCP1 Expression in Adipose Tissue from Cancer Cachexia Patients

Next, we explored the translational value of our findings and obtained eight samples of adipose tissue from cachectic cancer patients (Figure 7A). Despite the different anatomical location of the various adipose samples and regardless of the site of origin of the primary tumor, adipose tissue from cachectic patients exhibited morphologic features of atrophy: individual fat cells were reduced in size, had lost much of their cytoplasm, and showed a rounded or epithelioid appearance (Sternberg, 2006) (Figure 7B). In contrast, intestinal adipose tissue from patients with colon cancer, but no cachexia, appeared normal, with big adipocytes and small nuclei and being rich in lipids (Figure 7B). Importantly, a positive UCP1

**Figure 4. Role of Inflammation and IL-6 in the Pathophysiology of WAT Browning in Cachexia**

(A) Tumor weight in mice in the graft model with C26 colon cancer cells proficient or deficient for IL-6 (12 weeks old, n = 7 per condition).

(B and C) Changes in body (B) and organ (C) weight of mice in (A).

(D) Western blot analysis of UCP1 protein levels in axillary WAT of mice in (A).

(E) Plasma IL-6 levels in mice in the graft model with C26/IL-6 proficient cells with stable incorporation of shIL-6 or control vector (12 weeks old, n = 6 per condition).

(F) Measurement of body weight of mice in (E).

(G) Representative images of UCP1 IHC staining of axillary WAT of mice in (E).

(H) Analysis of oxygen consumption rate in isolated axillary WAT of mice in (E).

(I) Measurement of total WAT mass by DXA scan in K5-SOS mice before and after treatment with rat anti-mouse IL-6 monoclonal antibody or vehicle (pre: 5 weeks old; post: 7 weeks old; n = 5 per condition and per time point).

(J) Representative images of H&E staining of axillary WAT of mice in (I).

(K and L) Changes in total body (K) and organ (L) weight in IL-6-receptor KO mice and littermate controls, in the graft model with melanoma B16 cells (10 weeks old, n = 6 per genotype).

(M) Western blot analysis of UCP1 protein levels in axillary WAT of mice in (K).

Data are presented as mean ± SEM (*p < 0.05; **p < 0.01; ***p < 0.001).

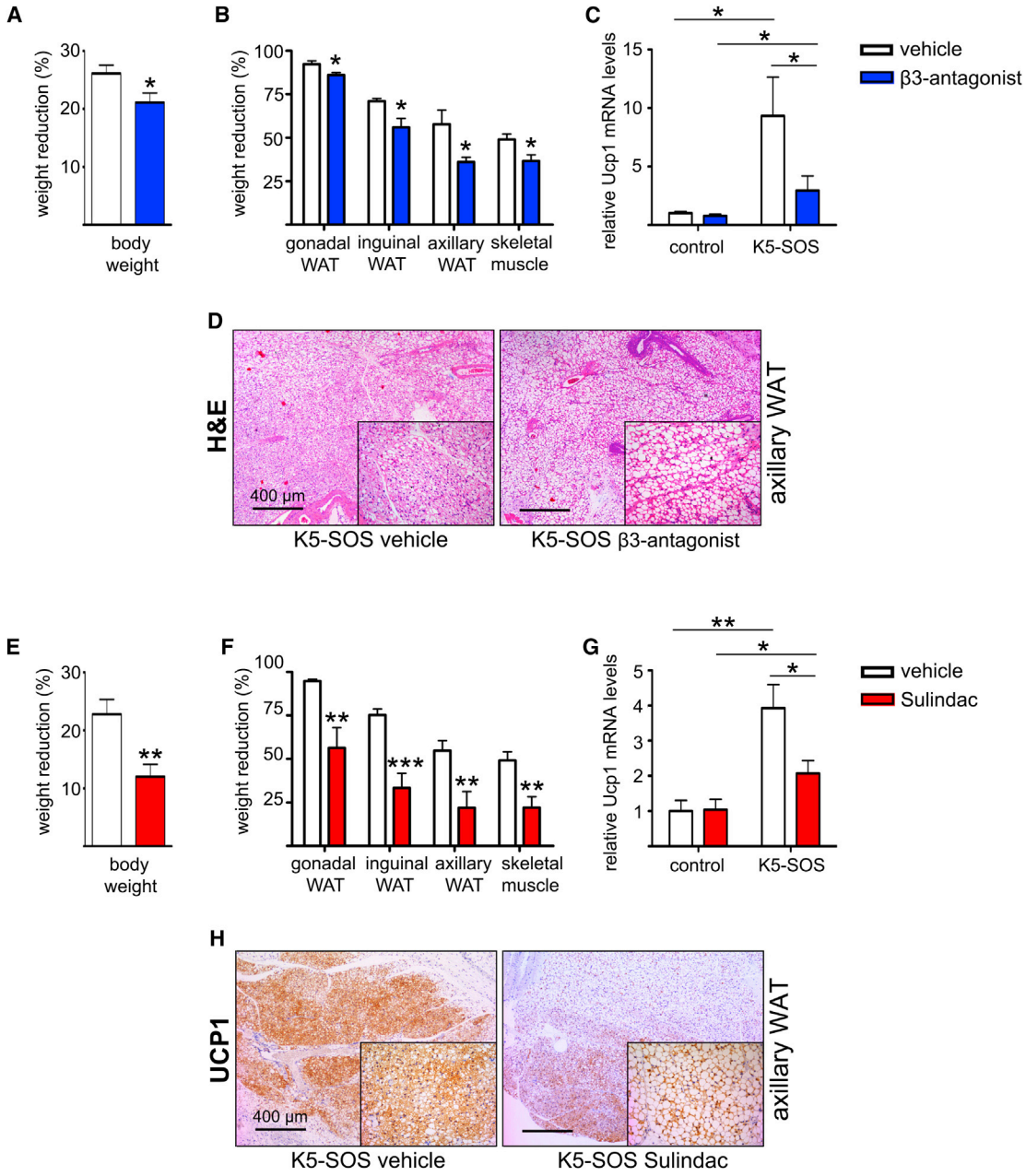


**Figure 6. Amelioration of Cachexia by β3-Adrenergic Receptor Antagonism or Anti-Inflammatory Treatment**

(A and B) Changes in total body weight (A) and organ weight (B) in K5-SOS mice treated with β3-AR antagonist or vehicle (7 weeks old, n ≥ 5 per genotype and per condition).

(C) Analysis of *Ucp1* gene expression levels in inguinal WAT in K5-SOS mice and littermate controls treated with β3-AR antagonist or vehicle.

(D) Representative images of H&E staining of axillary WAT in K5-SOS mice treated with β3-AR antagonist or vehicle.

(E and F) Changes in total body (E) and organ (F) weight in K5-SOS mice treated with sulindac or vehicle (7 weeks old, n ≥ 5 per genotype and per condition).

(G) Analysis of *Ucp1* gene expression levels in inguinal WAT in K5-SOS mice and littermate controls treated with sulindac or vehicle.

(H) Representative images of UCP1 IHC staining of axillary WAT in K5-SOS mice treated with sulindac or vehicle.

Data are presented as mean ± SEM (*$p < 0.05$; **$p < 0.01$; ***$p < 0.001$).

immunohistochemical staining was documented in seven out of eight samples analyzed (Figures 7A, 7C, and 7D). UCP1 staining was not evident in the only one adipose tissue sample from the pericardium observed, which may reflect differences in predisposition toward activation of the thermogenic program in adipose depots from anatomically distinct locations. Importantly, UCP1 staining was observed in samples from intestinal adipose tissue as well as fat surrounding the liver, kidney, and pancreas (Figure 7A). In contrast, 0/20 samples of intestinal adipose tissue from colon cancer patients without cachexia stained positive for

UCP1 (Figure 7C). These findings suggest that a common biological process may underlie adipocyte atrophy and UCP1 expression in cancer cachexia patients.

## DISCUSSION

Cachexia is a lethal syndrome and a frequent complication in patients suffering from malignancy or chronic cardiac, pulmonary, neurological, and infectious diseases. Originally conceived as a state of ''autocannibalism,'' in which the organism depletes its resources to provide nourishment to the tumor, cachexia is now described as an inflammatory and neuroendocrine response (Fearon et al., 2012). The severity of cachexia is commonly unrelated to tumor size or stage, with small tumors often responsible for severe wasting, as in the case of pancreatic and lung cancer (Tisdale, 2009). A combination of reduced food intake and abnormal metabolism characterizes the pathophysiology of cachexia and determines the negative energy and protein balance (Fearon et al., 2013). Unfortunately, improving nutritional intake has limited therapeutic potential, and available treatment options have no effect on the impaired metabolism (Fearon et al., 2013). Therefore, the prognosis of cachexia is currently very poor.

Here, we show that WAT browning represents an early and systemic event in cachexia pathophysiology and contributes to the increased energy expenditure and lipid mobilization. Increased energy expenditure was associated with activation of a thermogenic program in adipocytes characterized by increased mitochondrial content and uncoupling activity. The thermogenic activity was increased in interscapular BAT as well as in subcutaneous WAT depots. Interestingly, in subcutaneous WAT from cachectic mice there was a preferential increase in expression levels of brown-selective over beige-selective genes. This finding may seem unexpected, given the reported increased expression of beige-selective genes in subcutaneous WAT, when compared to interscapular BAT (Wu et al., 2012). However, these gene signatures were established in cell lines and validated in mice kept at ambient temperature, when the thermogenic program is not active in subcutaneous adipose depots. In fact, after activation of the thermogenic program, both inguinal and axillary WAT from cachectic mice displayed a gene expression profile that more closely resembled that of interscapular BAT. These data suggest that gene expression markers may be indicative of the activation state of the adipose tissue rather than its anatomical origin.

Activation of the thermogenic program in subcutaneous WAT occurs as a response to lower temperatures (Cousin et al., 1992). Although rectal temperature was decreased in cachectic mice, this occurred at a later clinical stage, when the cachectic phenotype was fully apparent. Several mechanisms account for hypothermia in terminal cachectic mice, including decreased insulating capacity due to loss of total WAT mass and decreased heat production due to reduced locomotor activity. Hypothermia in terminal mice may suggest that WAT browning is a compensatory mechanism. In contrast, WAT browning took place early in the progression of cachexia, preceding body weight loss, muscle atrophy, and hypothermia. Remarkably, different from cold-induced thermogenesis (Champigny and Ricquier, 1990), increasing the ambient temperature to thermoneutrality (30°C) did not suppress WAT browning in cachectic mice.

The role of UCP1 in metabolism goes beyond thermoregulation, as exemplified by diet- and β-adrenergic-induced thermogenesis, which are both active at thermoneutrality (Feldmann et al., 2009). To date, WAT browning has been described as a beneficial event, promoting weight loss and improving insulin sensitivity in metabolic diseases (Boström et al., 2012; Feldmann et al., 2009). However, here we show that WAT browning is deleterious in the context of cancer, contributing to energy dissipation and progression toward cachexia.

The pathophysiology of CAC is multifactorial, with many different mediators cooperating at different stages of the disease and in different cancer types (Fearon et al., 2012). We show that systemic inflammation plays a critical role in the pathogenesis of WAT browning. It is well known that inflammatory cytokines are pyrogenic and change the thermoneutrality set-point in the hypothalamus (Gordon, 2012). Experiments with IL-6 knockout mice have shown that IL-6 is required for maximal induction of UCP1 protein in subcutaneous fat depots in response to cold exposure (Knudsen et al., 2014). Circulating levels of IL-6 were increased in cachectic mice, and activation of IL-6 signaling was documented in adipose depots by phosphorylation of Stat3. The role of IL-6 was critical in the syngeneic graft model with C26 cancer cells, where genetic blockade of IL-6 production within the tumor prevented WAT browning and cachexia. Moreover, WAT browning was reduced in IL-6-R-KO mice implanted with B16 melanoma cells. Despite these facts, it cannot be excluded that other mediators in addition to IL-6 could stimulate WAT browning in cachectic mice. In this regard, the protection observed in IL-6-R-KO mice implanted with B16 melanoma cells was only partial, thus confirming that different mechanisms other than IL-6 signaling contribute to cachexia.

The mechanism by which IL-6 induces WAT browning in cachectic mice may involve alternative activation of macrophages (Mauer et al., 2014) and recruitment of β-adrenergic fibers (Nguyen et al., 2011). Indeed, surgical ablation experiments showed that the presence of an intact adrenergic innervation was essential for the complete induction of the thermogenic program in BAT of cachectic mice. Although it was not possible to perform surgical denervation of the subcutaneous WAT, results of β3-AR blockade support a role for sympathetic innervations in the pathogenesis of WAT browning in cachexia. In addition, in vitro experiments showed a direct effect of IL-6 on *Ucp1* expression in isolated adipocytes. Even if the effect was mild, chronically increased circulating IL-6 levels may induce thermogenesis in adipose tissue, either alone or in combination with other cytokines.

Circulating levels of IL-6 in patients with cancer correlate with weight loss and reduced survival (Moses et al., 2009; Scott et al., 1996). Blocking IL-6 in patients with CAC has been shown to ameliorate several symptoms and signs of cachexia, like fatigue, anorexia, and anemia, although it is ineffective upon loss of lean mass (Bayliss et al., 2011). Results with monoclonal anti-IL-6 antibody in the K5-SOS mouse model recapitulate the partial benefit observed in clinical trials and support the concept that treatment of cachexia in cancer patients must start early (Fearon et al., 2013). Due to the severity of commonly reported side effects associated with anti-IL-6 therapy (Berti et al., 2013), it

A

| sample | Primary cancer | Location of adipose tissue | UCP1 |
|---|---|---|---|
| 1 | Kaposi's sarcoma | Intestinal Fat | + |
| 2 | Melanoma | Intestinal Fat | + |
| 3 | Cholangiocarcinoma | Perihepatic Fat | + |
| 4 | Colon Adenocarcinoma | Pericardial Fat | - |
| 5 | Pancreatic Neuroendocrine Cancer | Intestinal Fat | + |
| 6 | Pleomorphic Carcinoma Lung | Unspecified Origin | + |
| 7 | Lung Adenocarcinoma | Perirenal Fat | + |
| 8 | Lung Adenocarcinoma | Peripancreatic Fat | + |

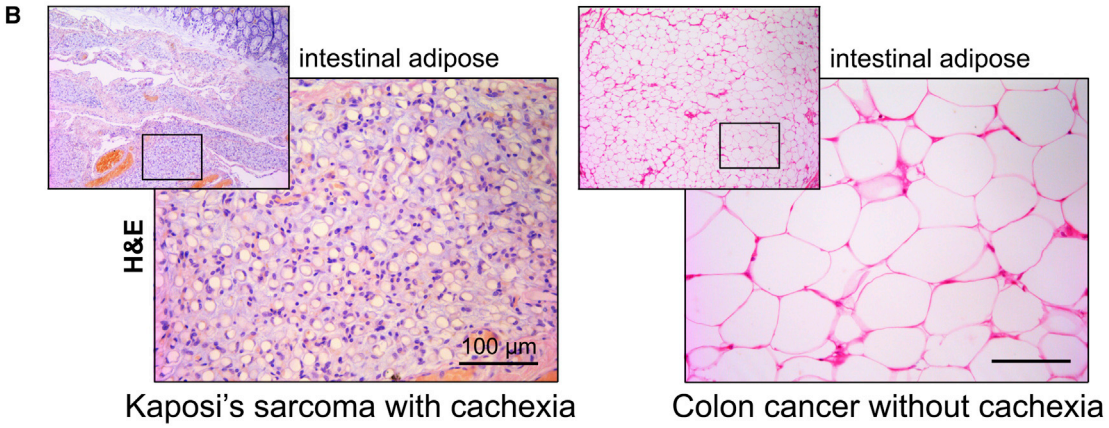


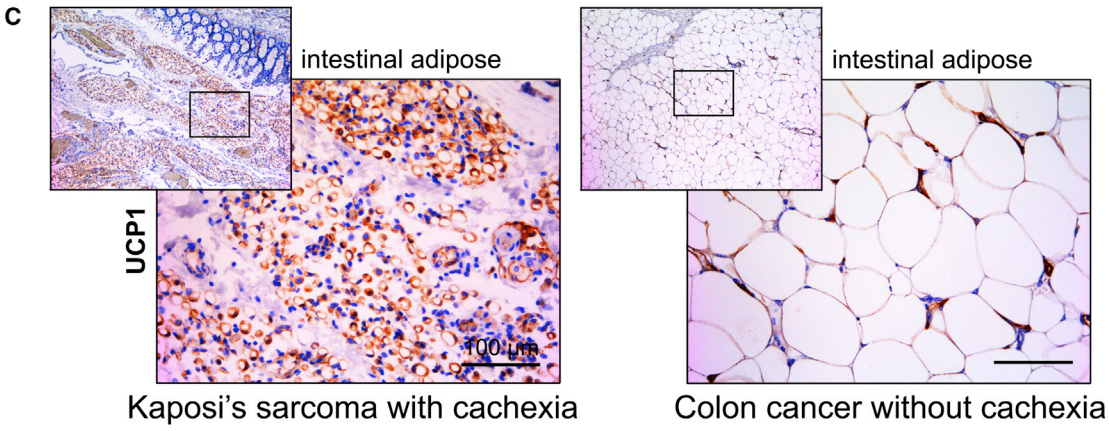


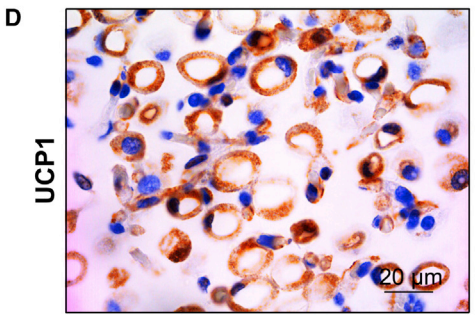


(legend on next page)

may prove difficult to prevent cachexia by IL-6 inhibition in early-stage cancer patients. Alternative preventive strategies may involve the use of β3-AR antagonists or, especially, nonsteroidal anti-inflammatory drugs, which were effective in experimental models. While both β3-AR blockade and sulindac treatment significantly reduced WAT browning in cachectic mice, other mechanisms could contribute to the therapeutic effect. Anti-inflammatory treatment has been shown to reduce the acute phase response and attenuate tumor progression in both preclinical models and patients with metastatic tumors (Lundholm et al., 1994). β3-AR blockade may protect against cachexia by means of decreased lipolysis (Tisdale, 2009), although β-adrenergic activation is only one of several pathways to account for increased lipolysis in CAC (Agustsson et al., 2007), and the presence of uniformly increased adrenergic activity in humans with CAC remains to be documented (Klein and Wolfe, 1990).

The induction of brown adipocytes in WAT depots of humans (Cypess et al., 2009; van Marken Lichtenbelt et al., 2009; Virtanen et al., 2009) has been shown recently to significantly affect overall energy balance (Yoneshiro et al., 2013). Human brown fat is composed of adipocytes similar to both classical interscapular brown adipocytes (Cypess et al., 2013; Jespersen et al., 2013; Lidell et al., 2013) and mouse white adipocytes converted into brown (Sharp et al., 2012; Wu et al., 2012). Moreover, a recent imaging study showed increased metabolic activity of BAT in PET-CTs of cancer patients (Huang et al., 2011). We have shown a switch from white to brown adipocytes in WAT of mice with CAC. WAT browning, together with enhanced thermogenesis in interscapular BAT, contributed to increased systemic energy expenditure. Also, preventing WAT browning by means of β3-AR antagonists or nonsteroidal anti-inflammatory drugs ameliorated the wasting process. The observation of increased UCP1 staining in adipose tissue from cachectic cancer patients indicates that adipocyte atrophy may be associated with increased thermogenic activity in human cancer cachexia. These data suggest that inhibition of WAT browning represents a promising approach to ameliorate the severity of cachexia in cancer patients.

## EXPERIMENTAL PROCEDURES

### Mice and Treatments

Mouse strains employed in this study have been previously described: Kras-pancreatic cancer GEMM (Hingorani et al., 2005), Kras-lung cancer GEMM (Puyol et al., 2010), K5-SOS mice (Sibilia et al., 2000), and IL-6-R-KO mice (McFarland-Mancini et al., 2010). All studies were performed with littermates of the same genetic background as controls. For the hepatic carcinogen model, 15-day-old mice on a mixed C57BL/6/129 background were injected intraperitoneally (i.p.) with 25 mg/kg DEN (Sigma-Aldrich). LLC cells ($4 \times 10^6$) or B16 melanoma cells ($2 \times 10^6$) were injected subcutaneously at dorsum just below the neck in C57Bl/6 mice. C26 cells ($1 \times 10^6$) were injected subcutaneously into the right flank of Balb/C × DBA1 hybrids. Mice used for injection of tumor cells as well as control animals were 10–12 weeks of age. Xenograft experiments were conducted in accordance with institutional guidelines of the CNIO (Protocol PA34/2012). Chow (D8604, Harlan) and 45% high-fat diet (D12451, Research Diets) were used in this study. For the thermoneutrality experiment, mice were introduced in the 30°C environment 1 week after weaning (4 weeks old) and housed with four mice per cage. Mice were acclimatized for 1 week prior to monitoring. Rat anti-mouse IL-6 monoclonal antibody (clone: MP5-20F3) was administered i.p. (five doses of 200 μg each, once each 3 days). The β3-AR antagonist SR59230A (Sigma-Aldrich; 3 mg/kg body weight per day) was administered through osmotic minipumps (Alzet). Sulindac (Sigma-Aldrich) was administered in drinking water (180 mg/l). Full methods are described in the Supplemental Experimental Procedures.

### Human Tumor Samples

After patients' informed consent had been obtained, excess tissues from resected pancreatic carcinomas were xenografted at Hospital de Madrid - Centro Integral Oncologico Clara Campal (FHM.06.10 "Establishment of bank for tumors and healthy tissue in patients with cancer") under the indicated Institutional Review Board approved protocols.

### qRT-PCR/Immunoblot Analysis

Quantitative RT-PCR reactions were performed using GoTaq RT-qPCR Master Mix (Promega) and Eppendorf fluorescence thermocyclers (Eppendorf). The 2-ΔΔCT method was used to quantify amplified fragments. Expression levels were normalized using two housekeeping genes (Actin and Gapdh). Primer sequences will be provided on request. Immunoblot analysis was performed using standard protocols and the following antibodies: mouse monoclonal anti-Actin (Sigma-Aldrich, A4700), rabbit polyclonal anti-ATGL (Cell Signaling Technology, #2138), rabbit monoclonal anti-GAPDH (Cell Signaling Technology, #2118), rabbit polyclonal anti-HSL (Cell Signaling Technology, #4107), rabbit monoclonal anti-NDUFS1 (Abcam, ab157221), rabbit polyclonal anti-p38α MAP-Kinase (Cell Signaling Technology, #9218), rabbit polyclonal anti-Phospho-HSL (Cell Signaling Technology, #4126), rabbit polyclonal anti-Phospho-p38α MAP-Kinase (Thr180/182; Cell Signaling Technology, #9211), rabbit polyclonal anti-Phospho-STAT3 (Tyr705; Cell Signaling Technology, #9131), rabbit polyclonal anti-STAT3 (Cell Signaling Technology, #9132), rabbit polyclonal anti-UCP1 (Abcam, ab10983), mouse monoclonal anti-Vinculin (Sigma-Aldrich, V9131).

### Oxygen Consumption Rate

Oxygen consumption rates (OCRs) in homogenized adipose tissue depots were analyzed by high-resolution respirometry (Oxygraph 2k, Oroboros Instruments) using glycerol-3-phosphate as substrate. Electron transfer via complex I in the respiratory chain was blocked by the addition of rotenone.

### Indirect Calorimetric Studies

To measure $O_2$ consumption, $CO_2$ production, food intake, and spontaneous motility, mice were housed in metabolic cages (LabMaster, TSE Systems GmbH). Animals were familiarized to single housing for at least 3 days prior to monitoring.

### IL-6 Knockdown in C26 Tumors

IL-6 expression in C26 cells was knocked down with lentiviral constructs from the MISSION shRNA Library (Sigma-Aldrich). Transduced cells were selected with puromycin, single-cell clones were derived, and the clones were tested by qPCR and ELISA for reduced IL-6 expression after in vitro IL-1β stimulation. The C26 tumors with the stably integrated IL-6 shRNA construct or vector control were implanted into mice as outlined above.

### Dual Energy X-Ray Absorptiometry Analysis

Whole-body fat mass density was measured by a PIXImus2 scanner according to the manufacturer's protocol (Lunar Corporation).

### Surgical Denervation

Mice (4 weeks old) underwent bilateral surgical denervation of the interscapular BAT under isoflurane anesthesia. A transverse incision was made just

**Figure 7. UCP1 Expression in Atrophic WAT from Cancer Cachexia Patients**

(A) Origin of the primary tumor, anatomical location of the WAT, and UCP1 IHC status in the human cancer cachexia samples analyzed.
(B and C) Representative images of H&E (B) and UCP1 IHC (C) staining of intestinal WAT from cancer patients with or without cachexia.
(D) Magnification of UCP1 IHC staining in intestinal WAT from the cachectic patient in (C).

anterior to the BAT, and the organ was exposed. After carefully moving the BAT outward from the surrounding muscle and white adipose tissue, the sympathetic chains innervating the organ were exposed. Denervation was performed by isolation and resection with scissors of the five branches of the left and right intercostal nerve bundles, without disrupting the blood circulation. In sham-operated mice, the sympathetic chains innervating BAT were exposed but not resected. Mice were sacrificed 1 week after surgery.

### Human Cancer Cachexia Slides

Paraffin sections of adipose tissue from cancer patients were obtained at tumor biopsy or at necropsy. The samples were provided by the CNIO Tumor Bank, CNIO, Madrid, and The Biobank of Hospital Clínic - IDIBAPS, Barcelona, in accordance with the ethical guidelines of the Helsinki Declaration.

### Statistical Analysis

Results are presented as mean ± SEM. p value was calculated using Student's t test.

## SUPPLEMENTAL INFORMATION

Supplemental Information includes Supplemental Experimental Procedures and seven figures and can be found with this article online at http://dx.doi.org/10.1016/j.cmet.2014.06.011.

## AUTHOR CONTRIBUTIONS

M.P. conceived the hypothesis, designed and performed experiments, and wrote the manuscript. M. Schweiger performed lipolysis, metabolic chambers, and thermoneutrality experiments and helped edit the manuscript. R.S. performed western blot analysis and mitochondrial DNA and OCR measurements. R.C.-O. performed NMR experiments and helped edit the manuscript. M.T. performed analysis in the C26 transplant model. J.A. performed IL-6 shRNA knockdown. M. Swarbrick performed IHC and mitochondrial tests. S.R.-J. provided the anti-IL-6 antibody. M.R. provided IL-6-R-KO mice and helped edit the manuscript. G.R. and R.Z. designed experiments and helped edit the manuscript. E.F.W. secured funding, supervised the project, and wrote the manuscript.

## ACKNOWLEDGMENTS

We thank the members of the Wagner lab for help and critical reading; S. Leceta, G. Luque, and G. Medrano for help with mouse procedures; and N. Djouder, M.A. Fawal, C. Heeschen, M. López, and M. Serrano for support and advice. We also thank C. Ambrogio, S. García, and M. Barbacid for Cancer GEMMs, E. Lopez-Guadamillas for 3T3-L1/Cebp/β cells, R.W. Hamacher for carcinogen-treated mice, M. Hidalgo for xenograft samples, the CNIO Tumor Bank and IDIBAPS Biobank, Barcelona for human samples, and M. Morente for expert pathological analysis. S.R.-J. was supported by the Deutsche Forschungsgemeinschaft, Germany (SFB654, project C5). G.R. was funded by Paul Ainsworth and the Dawkins family donations to the Garvan Foundation. The R.Z. laboratory is supported by the Fondation Leducq (12CVD04), an ERC-Advanced grant (LIPOCHEX Nr. 340896), the Z136 Wittgenstein Award, and the F30 SFB LIPOTOX from the Austrian Science Fund. The E.F.W. laboratory is supported by the Banco Bilbao Vizcaya Argentaria Foundation (F-BBVA), a grant from the Spanish Ministry of Economy (BFU2012-40230), and an ERC-Advanced grant (ERC-FCK/2008/37). M.P. was funded in part by a Caja-Navarra fellowship and the Union for International Cancer Control.

Received: December 18, 2013
Revised: April 28, 2014
Accepted: June 4, 2014
Published: July 17, 2014

## REFERENCES

Agustsson, T., Rydén, M., Hoffstedt, J., van Harmelen, V., Dicker, A., Laurencikiene, J., Isaksson, B., Permert, J., and Arner, P. (2007). Mechanism of increased lipolysis in cancer cachexia. Cancer Res. *67*, 5531–5537.

Bayliss, T.J., Smith, J.T., Schuster, M., Dragnev, K.H., and Rigas, J.R. (2011). A humanized anti-iL-6 antibody (ALD518) in non-small cell lung cancer. Expert Opin. Biol. Ther. *11*, 1663–1668.

Berti, A., Boccalatte, F., Sabbadini, M.G., and Dagna, L. (2013). Assessment of tocilizumab in the treatment of cancer cachexia. J. Clin. Oncol. *31*, 2970.

Blum, D., Omlin, A., Baracos, V.E., Solheim, T.S., Tan, B.H., Stone, P., Kaasa, S., Fearon, K., and Strasser, F.; European Palliative Care Research Collaborative (2011). Cancer cachexia: a systematic literature review of items and domains associated with involuntary weight loss in cancer. Crit. Rev. Oncol. Hematol. *80*, 114–144.

Boström, P., Wu, J., Jedrychowski, M.P., Korde, A., Ye, L., Lo, J.C., Rasbach, K.A., Boström, E.A., Choi, J.H., Long, J.Z., et al. (2012). A PGC1-α-dependent myokine that drives brown-fat-like development of white fat and thermogenesis. Nature *481*, 463–468.

Cannon, B., and Nedergaard, J. (2004). Brown adipose tissue: function and physiological significance. Physiol. Rev. *84*, 277–359.

Cao, L., Choi, E.Y., Liu, X., Martin, A., Wang, C., Xu, X., and During, M.J. (2011). White to brown fat phenotypic switch induced by genetic and environmental activation of a hypothalamic-adipocyte axis. Cell Metab. *14*, 324–338.

Champigny, O., and Ricquier, D. (1990). Effects of fasting and refeeding on the level of uncoupling protein mRNA in rat brown adipose tissue: evidence for diet-induced and cold-induced responses. J. Nutr. *120*, 1730–1736.

Cousin, B., Cinti, S., Morroni, M., Raimbault, S., Ricquier, D., Pénicaud, L., and Casteilla, L. (1992). Occurrence of brown adipocytes in rat white adipose tissue: molecular and morphological characterization. J. Cell Sci. *103*, 931–942.

Cypess, A.M., Lehman, S., Williams, G., Tal, I., Rodman, D., Goldfine, A.B., Kuo, F.C., Palmer, E.L., Tseng, Y.H., Doria, A., et al. (2009). Identification and importance of brown adipose tissue in adult humans. N. Engl. J. Med. *360*, 1509–1517.

Cypess, A.M., White, A.P., Vernochet, C., Schulz, T.J., Xue, R., Sass, C.A., Huang, T.L., Roberts-Toler, C., Weiner, L.S., Sze, C., et al. (2013). Anatomical localization, gene expression profiling and functional characterization of adult human neck brown fat. Nat. Med. *19*, 635–639.

Das, S.K., Eder, S., Schauer, S., Diwoky, C., Temmel, H., Guertl, B., Gorkiewicz, G., Tamilarasan, K.P., Kumari, P., Trauner, M., et al. (2011). Adipose triglyceride lipase contributes to cancer-associated cachexia. Science *333*, 233–238.

Fearon, K.C., Glass, D.J., and Guttridge, D.C. (2012). Cancer cachexia: mediators, signaling, and metabolic pathways. Cell Metab. *16*, 153–166.

Fearon, K., Arends, J., and Baracos, V. (2013). Understanding the mechanisms and treatment options in cancer cachexia. Nat Rev Clin Oncol *10*, 90–99.

Feldmann, H.M., Golozoubova, V., Cannon, B., and Nedergaard, J. (2009). UCP1 ablation induces obesity and abolishes diet-induced thermogenesis in mice exempt from thermal stress by living at thermoneutrality. Cell Metab. *9*, 203–209.

Gordon, C.J. (2012). Thermal physiology of laboratory mice: Defining thermoneutrality. J. Therm. Biol. *37*, 654–685.

Harms, M., and Seale, P. (2013). Brown and beige fat: development, function and therapeutic potential. Nat. Med. *19*, 1252–1263.

Hingorani, S.R., Wang, L., Multani, A.S., Combs, C., Deramaudt, T.B., Hruban, R.H., Rustgi, A.K., Chang, S., and Tuveson, D.A. (2005). Trp53R172H and KrasG12D cooperate to promote chromosomal instability and widely metastatic pancreatic ductal adenocarcinoma in mice. Cancer Cell *7*, 469–483.

Holroyde, C.P., Skutches, C.L., Boden, G., and Reichard, G.A. (1984). Glucose metabolism in cachectic patients with colorectal cancer. Cancer Res. *44*, 5910–5913.

Huang, Y.C., Chen, T.B., Hsu, C.C., Li, S.H., Wang, P.W., Lee, B.F., Kuo, C.Y., and Chiu, N.T. (2011). The relationship between brown adipose tissue activity and neoplastic status: an (18)F-FDG PET/CT study in the tropics. Lipids Health Dis. *10*, 238.

Jespersen, N.Z., Larsen, T.J., Peijs, L., Daugaard, S., Homøe, P., Loft, A., de Jong, J., Mathur, N., Cannon, B., Nedergaard, J., et al. (2013). A classical brown adipose tissue mRNA signature partly overlaps with brite in the supraclavicular region of adult humans. Cell Metab. *17*, 798–805.

Klein, S., and Wolfe, R.R. (1990). Whole-body lipolysis and triglyceride-fatty acid cycling in cachectic patients with esophageal cancer. J. Clin. Invest. *86*, 1403–1408.

Knudsen, J.G., Murholm, M., Carey, A.L., Biensø, R.S., Basse, A.L., Allen, T.L., Hidalgo, J., Kingwell, B.A., Febbraio, M.A., Hansen, J.B., and Pilegaard, H. (2014). Role of IL-6 in exercise training- and cold-induced UCP1 expression in subcutaneous white adipose tissue. PLoS ONE *9*, e84910.

Lee, Y.H., Petkova, A.P., Mottillo, E.P., and Granneman, J.G. (2012). In vivo identification of bipotential adipocyte progenitors recruited by β3-adrenoceptor activation and high-fat feeding. Cell Metab. *15*, 480–491.

Lidell, M.E., Betz, M.J., Dahlqvist Leinhard, O., Heglind, M., Elander, L., Slawik, M., Mussack, T., Nilsson, D., Romu, T., Nuutila, P., et al. (2013). Evidence for two types of brown adipose tissue in humans. Nat. Med. *19*, 631–634.

Loncar, D., Bedrica, L., Mayer, J., Cannon, B., Nedergaard, J., Afzelius, B.A., and Svajger, A. (1986). The effect of intermittent cold treatment on the adipose tissue of the cat. Apparent transformation from white to brown adipose tissue. J. Ultrastruct. Mol. Struct. Res. *97*, 119–129.

Lundholm, K., Gelin, J., Hyltander, A., Lönnroth, C., Sandström, R., Svaninger, G., Körner, U., Gülich, M., Kärrefors, I., Norli, B., et al. (1994). Anti-inflammatory treatment may prolong survival in undernourished patients with metastatic solid tumors. Cancer Res. *54*, 5602–5606.

Mauer, J., Chaurasia, B., Goldau, J., Vogt, M.C., Ruud, J., Nguyen, K.D., Theurich, S., Hausen, A.C., Schmitz, J., Brönneke, H.S., et al. (2014). Signaling by IL-6 promotes alternative activation of macrophages to limit endotoxemia and obesity-associated resistance to insulin. Nat. Immunol. *15*, 423–430.

McFarland-Mancini, M.M., Funk, H.M., Paluch, A.M., Zhou, M., Giridhar, P.V., Mercer, C.A., Kozma, S.C., and Drew, A.F. (2010). Differences in wound healing in mice with deficiency of IL-6 versus IL-6 receptor. J. Immunol. *184*, 7219–7228.

Moses, A.G., Maingay, J., Sangster, K., Fearon, K.C., and Ross, J.A. (2009). Pro-inflammatory cytokine release by peripheral blood mononuclear cells from patients with advanced pancreatic cancer: relationship to acute phase response and survival. Oncol. Rep. *21*, 1091–1095.

Nguyen, K.D., Qiu, Y., Cui, X., Goh, Y.P., Mwangi, J., David, T., Mukundan, L., Brombacher, F., Locksley, R.M., and Chawla, A. (2011). Alternatively activated macrophages produce catecholamines to sustain adaptive thermogenesis. Nature *480*, 104–108.

Ortega-Molina, A., Efeyan, A., Lopez-Guadamillas, E., Muñoz-Martin, M., Gómez-López, G., Cañamero, M., Mulero, F., Pastor, J., Martinez, S., Romanos, E., et al. (2012). Pten positively regulates brown adipose function, energy expenditure, and longevity. Cell Metab. *15*, 382–394.

Puyol, M., Martín, A., Dubus, P., Mulero, F., Pizcueta, P., Khan, G., Guerra, C., Santamaría, D., and Barbacid, M. (2010). A synthetic lethal interaction between K-Ras oncogenes and Cdk4 unveils a therapeutic strategy for non-small cell lung carcinoma. Cancer Cell *18*, 63–73.

Scott, H.R., McMillan, D.C., Crilly, A., McArdle, C.S., and Milroy, R. (1996). The relationship between weight loss and interleukin 6 in non-small-cell lung cancer. Br. J. Cancer *73*, 1560–1562.

Shabalina, I.G., Petrovic, N., de Jong, J.M., Kalinovich, A.V., Cannon, B., and Nedergaard, J. (2013). UCP1 in brite/beige adipose tissue mitochondria is functionally thermogenic. Cell Rep *5*, 1196–1203.

Sharp, L.Z., Shinoda, K., Ohno, H., Scheel, D.W., Tomoda, E., Ruiz, L., Hu, H., Wang, L., Pavlova, Z., Gilsanz, V., and Kajimura, S. (2012). Human BAT possesses molecular signatures that resemble beige/brite cells. PLoS ONE *7*, e49452.

Sibilia, M., Fleischmann, A., Behrens, A., Stingl, L., Carroll, J., Watt, F.M., Schlessinger, J., and Wagner, E.F. (2000). The EGF receptor provides an essential survival signal for SOS-dependent skin tumor development. Cell *102*, 211–220.

Sternberg, S.S. (2006). Histology for Pathologists. (Philadelphia: Lippincott Williams & Wilkins).

Summermatter, S., Santos, G., Pérez-Schindler, J., and Handschin, C. (2013). Skeletal muscle PGC-1α controls whole-body lactate homeostasis through estrogen-related receptor α-dependent activation of LDH B and repression of LDH A. Proc. Natl. Acad. Sci. USA *110*, 8738–8743.

Tang, W., Zeve, D., Seo, J., Jo, A.Y., and Graff, J.M. (2011). Thiazolidinediones regulate adipose lineage dynamics. Cell Metab. *14*, 116–122.

Tisdale, M.J. (2002). Cachexia in cancer patients. Nat. Rev. Cancer *2*, 862–871.

Tisdale, M.J. (2009). Mechanisms of cancer cachexia. Physiol. Rev. *89*, 381–410.

Tsoli, M., Moore, M., Burg, D., Painter, A., Taylor, R., Lockie, S.H., Turner, N., Warren, A., Cooney, G., Oldfield, B., et al. (2012). Activation of thermogenesis in brown adipose tissue and dysregulated lipid metabolism associated with cancer cachexia in mice. Cancer Res. *72*, 4372–4382.

van Marken Lichtenbelt, W.D., Vanhommerig, J.W., Smulders, N.M., Drossaerts, J.M., Kemerink, G.J., Bouvy, N.D., Schrauwen, P., and Teule, G.J. (2009). Cold-activated brown adipose tissue in healthy men. N. Engl. J. Med. *360*, 1500–1508.

Vegiopoulos, A., Müller-Decker, K., Strzoda, D., Schmitt, I., Chichelnitskiy, E., Ostertag, A., Berriel Diaz, M., Rozman, J., Hrabe de Angelis, M., Nüsing, R.M., et al. (2010). Cyclooxygenase-2 controls energy homeostasis in mice by de novo recruitment of brown adipocytes. Science *328*, 1158–1161.

Villarroya, F., and Vidal-Puig, A. (2013). Beyond the sympathetic tone: the new brown fat activators. Cell Metab. *17*, 638–643.

Virtanen, K.A., Lidell, M.E., Orava, J., Heglind, M., Westergren, R., Niemi, T., Taittonen, M., Laine, J., Savisto, N.J., Enerbäck, S., and Nuutila, P. (2009). Functional brown adipose tissue in healthy adults. N. Engl. J. Med. *360*, 1518–1525.

Waldén, T.B., Hansen, I.R., Timmons, J.A., Cannon, B., and Nedergaard, J. (2012). Recruited vs. nonrecruited molecular signatures of brown, "brite," and white adipose tissues. Am. J. Physiol. Endocrinol. Metab. *302*, E19–E31.

Wang, Q.A., Tao, C., Gupta, R.K., and Scherer, P.E. (2013). Tracking adipogenesis during white adipose tissue development, expansion and regeneration. Nat. Med. *19*, 1338–1344.

Wu, J., Boström, P., Sparks, L.M., Ye, L., Choi, J.H., Giang, A.H., Khandekar, M., Virtanen, K.A., Nuutila, P., Schaart, G., et al. (2012). Beige adipocytes are a distinct type of thermogenic fat cell in mouse and human. Cell *150*, 366–376.

Wu, J., Cohen, P., and Spiegelman, B.M. (2013). Adaptive thermogenesis in adipocytes: is beige the new brown? Genes Dev. *27*, 234–250.

Yoneshiro, T., Aita, S., Matsushita, M., Kayahara, T., Kameya, T., Kawai, Y., Iwanaga, T., and Saito, M. (2013). Recruited brown adipose tissue as an antiobesity agent in humans. J. Clin. Invest. *123*, 3404–3408.

Young, P., Arch, J.R., and Ashwell, M. (1984). Brown adipose tissue in the parametrial fat pad of the mouse. FEBS Lett. *167*, 10–14.

Zhou, X., Wang, J.L., Lu, J., Song, Y., Kwak, K.S., Jiao, Q., Rosenfeld, R., Chen, Q., Boone, T., Simonet, W.S., et al. (2010). Reversal of cancer cachexia and muscle wasting by ActRIIB antagonism leads to prolonged survival. Cell *142*, 531–543.